Anisotropic Vector Play Model and its Application in Magnetization Analysis

Matsuo, Tetsuji; Takahashi, Yasuhito; Fujiwara, Koji

Anisotropic Vector Play Model and Its Application in Magnetization Analysis

Tetsuji Matsuo[1], *Member, IEEE*, Yasuhito Takahashi[2], *Member, IEEE*, and Koji Fujiwara[2], *Member, IEEE*

[1]Graduate School of Engineering Kyoto University, Kyoto 615-8510, Japan
[2]Department of Electrical Engineering, Doshisha University, Kyotanabe 610-0321, Japan

Abstract— An anisotropic vector play model was developed by the superposition of scalar play models. An analytical identification method was derived for a uniaxially anisotropic term. Computed *BH* loops accurately reconstructed the measured anisotropic hysteretic characteristics of non-oriented silicon steel sheet. Its application to magnetization analysis by a physical magnetization model using multi-domain particles enhanced the prediction accuracy of the stress-dependent loss property.

***Keywords*— anisotropic vector hysteresis, identification, uniaxial anisotropy, mechanical stress**

I. Introduction

There exist several vector versions of hysteresis models, such as the Preisch model [1], [2], the Jiles-Atherton model [3], and the play model [4], [5], which have been applied to the magnetic field analysis [3], [6]. Among them, the play model is an accurate and efficient hysteresis model. Although the scalar play model is mathematically equivalent to the Preisach model [7], its computational cost is lower.

The play model contains two types of vector versions; one is the geometric extension of a scalar model, while the other is constructed by the superposition of scalar models [5]. The geometric model has been applied to magnetic field analysis [6] because it represents iron core properties more accurately and efficiently than the superposition model. The superposition model has a physics-based background, similar to the vector Preisach model [1]; therefore, it is used to identify the pinning field components from the measured *MH* loop to present a pinning field distribution to a physical magnetization model, such as the multi-domain particle model (MDPM) [8] (See Appendix for a brief explanation of magnetization model). The pinning field distribution is one of the key data for the MDPM. Assuming an isotropic pinning field distribution, the MDPM succeeded to predict the stress dependence of hysteresis loss without using measured data under mechanical stress [8]. As was revealed in [9], the stress dependence is caused by the stress-induced anisotropy. However, the isotropic pinning field distribution may be an insufficient approximation to be coupled with stress-induced anisotropy.

Using the equivalence to the Preisach model, an anisotropic vector play model of the superposition type can be constructed in the same manner as the anisotropic vector Preisach model proposed by Mayergoyz [1]. However, its identification method is complicated, making implementation difficult. This study aimed to develop a superposition-type anisotropic vector play model and its analytical identification method. It was applied to estimate the anisotropic pinning field distribution used in the MDPM.

Manuscript received April 1, 2015; revised May 15, 2015 and June 1, 2015; accepted July 1, 2015. Date of publication July 10, 2015; date of current version July 31, 2015. (Dates will be inserted by IEEE; "published" is the date the accepted preprint is posted on IEEE Xplore®; "current version" is the date the typeset version is posted on Xplore®). Corresponding author: T. Matsuo (e-mail: matsuo.tetsuji.5u@kyoto-u.ac.jp).

Color versions of one or more of the figures in this paper are available online at http://ieeexplore.ieee.org.

Digital Object Identifier (inserted by IEEE).

II. Anisotropic Vector Play Model

A. Anisotropic Vector Model Based on Superposition

A hysteretic function from input X to output Y is represented by a scalar play model as

$$Y = F(X) + \int_{+0}^{X_S} f(\zeta, p_\zeta(X))\, \mathrm{d}\zeta , \qquad (1)$$

where F and f represent single-valued functions called shape functions, and X_S indicates the saturation point. The play hysteron operator p_ζ having width ζ is given as

$$p_\zeta(X) = \max(\min(p_\zeta^0, X+\zeta), X-\zeta), \qquad (2)$$

where $p_{\zeta 0}$ indicates p_ζ at the previous time point.

A vector hysteresis model with uniaxial anisotropy is constructed by the superposition of scalar models [1] as

$$\boldsymbol{Y} = = \int_{-\pi/2}^{\pi/2} \boldsymbol{e}_\varphi [P_{20}(\boldsymbol{e}_\varphi \cdot \boldsymbol{X}) + P_{22}(\boldsymbol{e}_\varphi \cdot \boldsymbol{X}) \cos 2\varphi] \mathrm{d}\varphi , \qquad (3)$$

where $\boldsymbol{X}$ represents the input vector, $\boldsymbol{Y}$ represents the output vector, φ symbolizes the azimuth angle, $\boldsymbol{e}_\varphi$ represents the unit vector in the φ-direction, and P_{20} and P_{22} represent the scalar hysteretic functions given by the play or Preisach model.

The rotational hysteresis loss yielded by the vector model (3) saturates for a rotational input of large amplitude, which is unrealistic for the magnetic hysteresis of core materials. The isotropic vector model has an extended version to enhance the rotational loss property representation [1], [5]. Similarly, the anisotropic vector model (3) can be extended as:

$$\boldsymbol{Y} = = \int_{-\pi/2}^{\pi/2} \boldsymbol{e}_\varphi [P_{20}(|\boldsymbol{X}| \cos^{\frac{1}{n}} \psi) + P_{22}(|\boldsymbol{X}| \cos^{\frac{1}{n}} \psi) \cos 2\varphi] \mathrm{d}\varphi , \qquad (4)$$

where ψ denotes the angle between $\boldsymbol{X}$ and $\boldsymbol{e}_\varphi$. More precisely, $\cos^{1/n}\psi$ means $|\cos\psi|^{1/n}\mathrm{sign}(\cos\psi)$.

The unidirectional property of (3) and (4) along the φ-direction is given from measured data and represented as

$$Y_\varphi = P_{10}(X) + P_{12}(X)\cos 2\varphi \tag{5}$$

where P_{10} and P_{12} are isotropic and anisotropic hysteresis functions given by the play or Preisach model.

The input and output vectors ($\boldsymbol{X}$, $\boldsymbol{Y}$) can be either ($\boldsymbol{H}$, $\boldsymbol{B}$) or ($\boldsymbol{B}$, $\boldsymbol{H}$), where $\boldsymbol{H}$ indicates the magnetic field and $\boldsymbol{B}$ indicates the magnetic flux density. Although the H-input model is a natural choice for the play model, the B-input model is often used because it is favorable to the finite element method using magnetic vector potential, and the B-input model can more accurately represent the properties of silicon steel.

B. *Identification Method*

In [1], an identification method is given to analytically determine P_{20} from the measured P_{10} for the Preisach model. However, an analytical method that identifies P_{22} from P_{12} is not known. Therefore, this study derives an analytical identification method to determine P_{22} for the play model, which is applicable to the Preisach model.

The following function is defined for the identification:

$$T_{ik}(\zeta, p) = \begin{cases} F_{ik}(p) + \int_{+0}^{\zeta} f_{ik}(\xi, p)\,\mathrm{d}\xi & (0 < \zeta) \\ F_{ik}(p) & (\zeta = 0) \end{cases}, \tag{6}$$

where i = 1, 2 and k = 0, 2. T_{1k} is given from the shape functions F_{1k} and f_{1k} of P_{1k}. Using T_{1k}, F_{2k} and f_{2k} of P_{2k} are given as

$$f_{2k}(\zeta, p) = \frac{\partial T_{2k}(\zeta, p)}{\partial \zeta},\ F_{2k}(p) = T_{2k}(0, p), \tag{7}$$

where k = 0, 2 and

$$T_{2k}(\zeta, p) = \frac{1}{\pi}\int_0^{\pi/2} \tilde{T}_{1k}(\zeta\cos^{1/n}\varphi, p\cos^{1/n}\varphi)\mathrm{d}\varphi, \tag{8}$$

$$\tilde{T}_{10}(\zeta, p) = T_{10}(\zeta, p) + \frac{\zeta}{n}\frac{\partial T_{10}(\zeta, p)}{\partial \zeta} + \frac{p}{n}\frac{\partial T_{10}(\zeta, p)}{\partial p}, \tag{9}$$

$$\tilde{T}_{12}(\zeta, p) = 3T_{12}(\zeta, p) + \frac{\zeta}{n}\frac{\partial T_{12}(\zeta, p)}{\partial \zeta} + \frac{p}{n}\frac{\partial T_{12}(\zeta, p)}{\partial p}. \tag{10}$$

Equation (9) was derived in [1] and [5]. The derivation of (10) is given in the following subsection.

In the case of the vector Preisach model, T_{ik} is replaced by the corresponding Everett integral.

C. *Derivation of (10)*

As is derived in [1] (with n = 1), it is necessary for the unidirectional property of (4) to be identical to (5), such that

$$P_{1k}(X) = \int_{-\pi/2}^{\pi/2} \cos\psi\cos(k\psi)P_{2k}(X\cos^{1/n}\psi)\,\mathrm{d}\psi. \tag{11}$$

In the case of the vector play model of the superposition type, (11) is replaced by

$$T_{1k}(\zeta, p) = \int_{-\pi/2}^{\pi/2} \cos\psi\cos(k\psi)T_{2k}(\zeta\cos^{1/n}\psi, p\cos^{1/n}\psi)\,\mathrm{d}\psi. \tag{12}$$

For k = 0, the solution of integral equation (12) for T_{20} is given by (8) and (9). For k = 2, (12) can be rewritten as

$$T_{12}(\zeta, p) = \int_{-\pi/2}^{\pi/2} (2\cos^3\psi - \cos\psi)T_{22}(\zeta\cos^{1/n}\psi, p\cos^{1/n}\psi)\,\mathrm{d}\psi. \tag{13}$$

By setting

$$\zeta' = \zeta\cos^{1/n}\psi,\ p' = p\cos^{1/n}\psi, \tag{14}$$

it holds for a function $T(\zeta', p')$ that

$$\begin{aligned}
&\int_{-\pi/2}^{\pi/2} (\cos^3\psi - \cos\psi)(T + \frac{\zeta'}{n}\frac{\partial T}{\partial \zeta'} + \frac{p'}{n}\frac{\partial T}{\partial p'})\,\mathrm{d}\psi \\
&= -\int_{-\pi/2}^{\pi/2} \cos\psi\sin^2\psi(T + \frac{\zeta'}{n}\frac{\partial T}{\partial \zeta'} + \frac{p'}{n}\frac{\partial T}{\partial p'})\,\mathrm{d}\psi \\
&= \int_{-\pi/2}^{\pi/2} \cos\psi\sin\psi\frac{\mathrm{d}}{\mathrm{d}\psi}(T\cos\psi)\,\mathrm{d}\psi \\
&= \left[T\cos^2\psi\sin\psi\right]_{-\pi/2}^{\pi/2} - \int_{-\pi/2}^{\pi/2} (\cos^3\psi - \cos\psi\sin^2\psi)T\,\mathrm{d}\psi \\
&= -\int_{-\pi/2}^{\pi/2} (2\cos^3\psi - \cos\psi)T\,\mathrm{d}\psi
\end{aligned} \tag{15}$$

From (15), the following is obtained

$$\begin{aligned}
&\int_{-\pi/2}^{\pi/2} \cos^3\psi(3T + \frac{\zeta'}{n}\frac{\partial T}{\partial \zeta'} + \frac{p'}{n}\frac{\partial T}{\partial p'})\,\mathrm{d}\psi \\
&= \int_{-\pi/2}^{\pi/2} \cos\psi(2T + \frac{\zeta'}{n}\frac{\partial T}{\partial \zeta'} + \frac{p'}{n}\frac{\partial T}{\partial p'})\,\mathrm{d}\psi
\end{aligned} \tag{16}$$

Replacing $T(\zeta', p')$ by $T_{12}(\zeta'', p'') = T_{12}(\zeta'\cos^{1/n}\varphi, p'\cos^{1/n}\varphi)$ in (16) and using (8) and (10), we obtain

$$\begin{aligned}
&\int_{-\pi/2}^{\pi/2} (2\cos^3\psi - \cos\psi)T_{22}(\zeta', p')\,\mathrm{d}\psi \\
&= \frac{1}{\pi}\int_0^{\pi/2}\int_{-\pi/2}^{\pi/2} 2\cos\psi[2T_{12}(\zeta'', p'') + \frac{\zeta''}{n}\frac{\partial T_{12}}{\partial \zeta''} + \frac{p''}{n}\frac{\partial T_{12}}{\partial p''}]\mathrm{d}\psi\mathrm{d}\varphi \\
&\quad - \frac{1}{\pi}\int_0^{\pi/2}\int_{-\pi/2}^{\pi/2} \cos\psi[3T_{12}(\zeta'', p'') + \frac{\zeta''}{n}\frac{\partial T_{12}}{\partial \zeta''} + \frac{p''}{n}\frac{\partial T_{12}}{\partial p''}]\mathrm{d}\psi\mathrm{d}\varphi \\
&= \frac{1}{\pi}\int_{-\pi/2}^{\pi/2} \cos\psi\int_0^{\pi/2} [T_{12}(\zeta'\cos^{1/n}\varphi, p'\cos^{1/n}\varphi) \\
&\qquad + \frac{\zeta'\cos^{1/n}\varphi}{n}\frac{\partial T_{12}}{\partial \zeta''} + \frac{p'\cos^{1/n}\varphi}{n}\frac{\partial T_{12}}{\partial p''}]\mathrm{d}\varphi\mathrm{d}\psi \\
&= T_{12}(\zeta, p)
\end{aligned} \tag{17}$$

The last equation holds because this relation is the same as relations (8), (9), and (12) for T_{10} and T_{20} with k = 0. Thus, it is proven that T_{22} given by (8) and (10) satisfies (12).

III. Computational Results

A. *Vector Hysteretic Property of Silicon Steel Sheet*

A non-oriented (NO) silicon steel sheet JIS: 50A470 was measured along the rolling direction (RD) and transverse direction (TD). The B-input play model was used for this case. For simplicity, using the measured properties $H_{\mathrm{RD}}(B)$ and $H_{\mathrm{TD}}(B)$ in the RD and TD, $P_{10}(B)$ and $P_{12}(B)$ are approximated as

$$\begin{aligned}
P_{10}(B) &= [H_{\mathrm{RD}}(B) + H_{\mathrm{TD}}(B)]/2, \\
P_{12}(\mathrm{B}) &= [H_{\mathrm{RD}}(B) - H_{\mathrm{TD}}(B)]/2.
\end{aligned} \tag{18}$$

The developed identification method determines P_{20} and P_{22} from P_{10} and P_{12} above. Fig. 1 illustrates the reconstructed BH loops along the RD and TD with n = 1 and 5, where B_{S} (= X_{S}) is set to 1.8 T. The anisotropic property is accurately

represented. Fig. 2(a) presents the hysteresis loss per cycle along the RD and TD with n = 1, 3, 5. The alternating losses are accurately represented under the given parameter B_S.

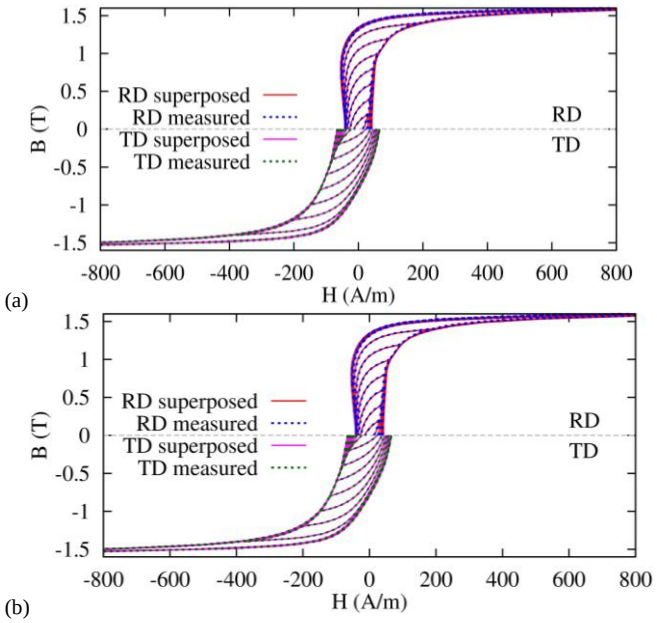

Fig. 1. BH loops simulated by the anisotropic vector play model: (a) n = 1 and (b) n = 5.

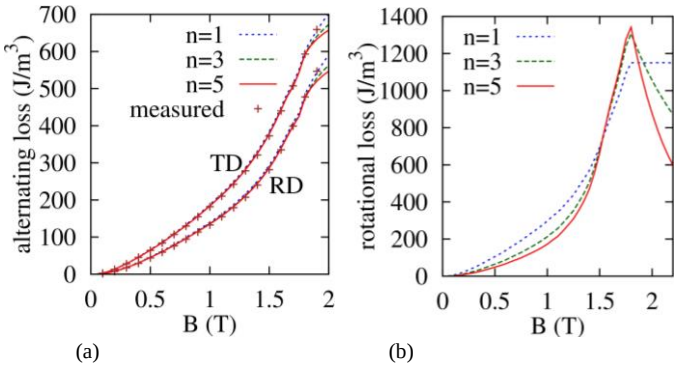

Fig. 2. Hysteresis losses per cycle: (a) alternating and (b) rotational losses.

Fig. 2(b) illustrates the rotational hysteresis loss per cycle with n = 1, 3, 5. The rotational loss saturates when n = 1, whereas it decreases for large B with n = 3 and 5. Thus, the simulated rotational hysteresis loss can be qualitatively controlled by the parameter n. To obtain a more accurate representation of the rotational hysteresis loss, a weighting function can be introduced, similar to the isotropic model discussed in [5].

B. Application in Magnetization Analysis

The MDPM [8] is a physical magnetization model, the multi-domain particle model (MDPM), which successfully predicts the increase in the hysteresis loss of silicon steel sheets owing to the compressive stress. The MDPM constitutes an assembly of 6-domain particles. The magnetization state in each particle is represented by the volume ratios r_j and the magnetization direction (θ_j, φ_j) of six domains (j = 1, …, 6); r_j and (θ_j, φ_j) are determined by locally minimizing the total magnetic energy comprising the Zeeman, anisotropy, magnetostatic, and magnetoelastic energies. The variation in the volume ratio r_j is resisted by a pinning field. See the Appendix for a brief explanation of the MDPM.

Assuming an isotropic pinning field, [8] provides the pinning field H_{pnj} working on r_j ($0 \le r_j \le 1$) as:

$$H_{pnj} = C\, r_j P_{20}(2r_j - 1), \tag{19}$$

where C is a constant and P_{20} is a function providing a pinning field distribution, which is represented by a scalar play model. P_{20} is estimated from the measured MH loops as follows.

Once the MH loops are unidirectionally measured under a stress-free condition, its anhysteretic component is subtracted from the MH loops to extract a unidirectional pinning field $P_{10}(m)$, where $m = M/M_S$ and M_S indicates spontaneous magnetization. P_{10} is approximated by the unidirectional property of a two-dimensional vector play model (3) (i.e., n = 1) without P_{12} and P_{22} terms. From (6)–(9), $P_{20}(m)$ is identified from $P_{10}(m)$. In each cell, m is replaced by $2r_j - 1$ in (19).

By replacing (19) with

$$H_{pnj} = C\, r_j[P_{20}(2r_j - 1) + P_{22}(2r_j - 1)\cos 2\varphi_j], \tag{20}$$

an anisotropic pinning field is represented to realize an anisotropic MDPM. Similarly, the pinning field distributions $P_{20}(m)$ and $P_{22}(m)$ are represented by the play model and identified from the measured MH loops along the RD and TD. Note that P_{20} and P_{22} are scalar play models. The vector magnetization property of the core material is constructed by the MDPM using the isotropic/anisotropic pinning field.

The stress-dependent properties of 50A470 were measured along the RD and TD using a stress-loading single-sheet tester [10]. The stress-dependent hysteresis loss is simulated using the isotropic and anisotropic MDPM. The isotropic MDPM for the RD (or TD) simulation uses the measured MH loops in the RD (TD) only, where the coefficient C in (19) is determined to adjust the simulated loss to the measured one in the RD (TD) around 1 to 1.2 T under the stress-free condition. The anisotropic MDPM uses the measured MH loops both in the RD and TD, an adjustment coefficient C in (20) is used for both the RD and TD simulation.

The material constants required for the computation represent the cubic anisotropy constant (K = 4.2 × 10^4 J/m^3) and magnetostriction constants (λ_{100} = 2.4 × 10^{-5}, λ_{111} = −9.5 × 10^{-6}), and $\mu_0 M_S$ = 2.07 T. Note that no measured data under mechanical stress are required for the MDPM to accurately predict the stress-dependent property.

Fig. 3 presents a comparison of the simulated and measured hysteresis losses per cycle with and without compressive stress of 40 MPa. The difference in the loss property between the RD and TD decreases under compressive stress. The isotropic MDPM overestimates the loss in the TD, whereas the anisotropic MDPM achieves good prediction accuracy coupled with stress-induced anisotropy. Fig. 4 depicts simulated BH loops, which roughly reconstruct measured loops. The property difference between the RD and TD becomes small under the stress because the stress-induced anisotropy is dominant.

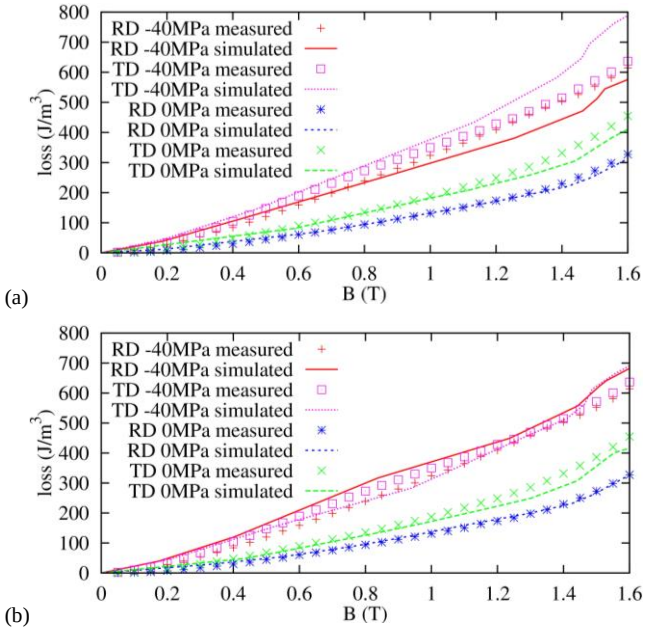

Fig. 3. Hysteresis losses under compressive stress predicted by the MDPM with (a) isotropic and (b) anisotropic pinning field distributions.

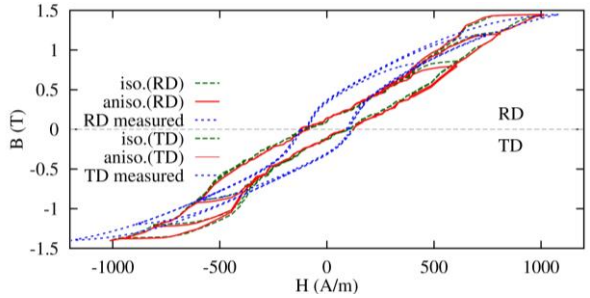

Fig. 4. BH loops under compressive stress of 40 MPa.

IV. Conclusion

A uniaxially anisotropic vector play model was developed, and its identification method was derived. The proposed method accurately reconstructed the *BH* loops of NO steel sheet in the RD and TD. The proposed method was applied to identify the anisotropic pinning field used in a physical magnetization model. The anisotropic pinning field improved the prediction of the stress-dependent loss property of NO steel sheet. To handle more complex anisotropy of steel sheets such as the grain-oriented silicon steel, a 2D/3D higher-order anisotropic vector model will be developed in future work.

Appendix

To represent the stress dependence of magnetization properties, several phenomenological models [11] and physical models [8], [12], [13] have been developed. To adjust fitting parameters, the phenomenological models require measured stress-dependent data, which are not always available, especially for various combinations of stress and magnetic field directions. The physical models succeeded to predict the stress dependence of the permeability and the shape of hysteresis loops. However, it is still an open problem to predict the stress dependence of hysteresis loss accurately.

The MDPM [8] is a physical macroscopic magnetization model developed by assembling mesoscopic particles at the crystal-grain scale. The magnetization state in each cell particle is represented by the volume ratios r_i and magnetization vectors ($\sin\theta_j\cos\phi_j$, $\sin\theta_j\sin\phi_j$, $\cos\theta_j$) (j = 1 … 6) of the six domains. These states are determined to locally minimize the total magnetic energy e, which comprises the Zeeman, crystalline anisotropy, magnetostatic, and magnetoelastic energies. Local minimization of e is achieved by solving the ordinary differential equations given as

$$\mathrm{d}\boldsymbol{x}/\mathrm{d}t = \boldsymbol{y},\ \mathrm{d}\boldsymbol{y}/\mathrm{d}t = -\partial e/\partial \boldsymbol{x} - \beta \boldsymbol{y}, \qquad (21)$$

where $\boldsymbol{x}$ consists of (θ_1, …, θ_6, ϕ_1, …, ϕ_6, r_1, …, r_5) and β denotes the damping factor. A local energy minimum is obtained by numerically integrating (21) until an equilibrium point is reached at which $\mathrm{d}\boldsymbol{x}/\mathrm{d}t = \mathrm{d}\boldsymbol{y}/\mathrm{d}t = 0$.

The pinning field is generated in each particle because of the domain-wall motion, which is modeled by the play model. The pinning field distribution is estimated based on the measured *MH* loops under stress-free conditions, whereas other model parameters were obtained from material constants (i.e., spontaneous magnetization, anisotropy constant, and magnetostriction constants). To add the pinning field, the $\partial e/\partial r_j$ term in (21) is replaced by $\partial e/\partial r_j + H_{\mathrm{pnj}}$, where the pinning field H_{pnj} is given as in (19) or (20).

References

[1] I.D. Mayergoyz, *Mathematical Models of Hysteresis and their Applications*, Elsevier, New York, 2003.

[2] E. Cardelli, E. Della Torre, A. Faba, "Numerical modeling of hysteresis in Si-Fe steels," *IEEE Trans. Magn.*, vol. 50, 7008004, Feb. 2014.

[3] K. Hoffmann, et.al, "A vector Jiles–Atherton model for improving the FEM convergence," *IEEE Trans. Magn.*, vol. 53, 7300304, Jun. 2017.

[4] A. Bergqvist, "Magnetic vector hysteresis model with dry friction-like pinning," *Physica B*, vol. 233, pp. 342-347, 1997.

[5] T. Matsuo, M. Shimasaki, "Two types of isotropic vector play models and their rotational hysteresis losses," *IEEE Trans. Magn.*, vol. 44, pp. 898-901, 2008 .

[6] J. Kitao, et al., "Loss calculation method considering hysteretic property with play model in finite element magnetic field analysis," *IEEE Trans. Magn.*, vol. 50, 7009304, 2014.

[7] S. Bobbio, G. Miano, C. Serpico, and C. Visone, "Models of magnetic hysteresis based on play and stop hysterons," *IEEE Trans. Magn.*, vol. 33, pp. 4417-4426, Nov. 1997.

[8] T. Matsuo, Y. Takahashi, K. Fujiwara. "Pinning field model using play hysterons for stress-dependent domain-structure model," *J. Magn. Magn. Mater.*, vol. 499, 166303, 2020.

[9] S. Ito, et al., "Simulation of the stress dependence of hysteresis loss using an energy-based domain model," *AIP Advances*, vol. 8, 047501, 2018.

[10] N. Kurita, et al., "Magnetic field analysis taking account of stress-dependent magnetic properties of non-oriented electrical steel sheets," Proc. 18th COMPUMAG, Sydney, Australia, PD7.7, 2011.

[11] P. Rasilo, et al., "Modeling of hysteresis losses in ferromagnetic laminations under mechanical stress," *IEEE Trans. Magn.*, vol. 52, 7300204, 2016.

[12] L. Daniel, M. Rekik, O. Hubert, "A multiscale model for magneto-elastic behaviour including hysteresis effects," *Arch. Appl. Mech.* vol. 84, pp. 1307–1323, 2014.

[13] D. Vanoost, et al., "Magnetic hysteresis at the domain scale of a multi-scale material model for magneto-elastic behavior," *J. Magn. Magn. Mater.*, vol. 414, pp. 168-179 Sept. 2016,